Electron-excited luminescence of SiC surfaces and interfaces

2004 J. Phys.: Condens. Matter 16 S1733

(http://iopscience.iop.org/0953-8984/16/17/015)

INSTITUTE OF PHYSICS PUBLISHING JOURNAL OF PHYSICS: CONDENSED MATTER

J. Phys.: Condens. Matter **16** (2004) S1733–S1754 PII: S0953-8984(04)65085-5

Electron-excited luminescence of SiC surfaces and interfaces

L J Brillson[1], S Tumakha[1], R S Okojie[1,2], M Zhang[1,3] and P Pirouz[1,3]

[1] The Ohio State University, 205 Dreese Laboratory, 2015 Neil Avenue, Columbus, OH 43210-1272, USA
[2] NASA Glenn Research Center, 21000 Brookpark Road, M/S 77-1, Cleveland, OH 44135, USA
[3] Department of Materials Science and Engineering, Case Western Reserve University, Cleveland, OH 44106, USA

E-mail: Brillson.1@osu.edu

Received 23 June 2003
Published 16 April 2004
Online at stacks.iop.org/JPhysCM/16/S1733
DOI: 10.1088/0953-8984/16/17/015

Abstract

Recent advances in probing the electronic structure of SiC with electron-excited luminescence techniques reveal the presence of localized electronic states near its surfaces and interfaces. These localized states form not only as a result of interface chemical bonding but also due to the formation of new lattice polytypes. Such electronic features are sensitive to the conditions under which the SiC is processed, as well as the application of electrical or mechanical stress. These localized changes on a nanometre scale provide a new perspective to Schottky barrier formation, band alignment, and polytypism in SiC as well as its performance in electronic devices.

(Some figures in this article are in colour only in the electronic version)

1. Introduction

The wide-band-gap semiconductor SiC possesses physical properties that are of high value for next-generation microelectronics [1]. SiC's large energy gap results in a very high resistance to electrical breakdown, an enabling feature of high-power transistors. Again because of its high band gap, as well as its high melting point, SiC can function electronically under high-temperature conditions. Furthermore, its high thermal conductivity renders SiC a desirable template for epitaxial growth of other high-power electronic materials such as GaN. As with other semiconductors, the Schottky barriers and heterojunction band offsets of SiC with other materials depend on local charge transfer at their interfaces [2], In turn, this charge transfer depends sensitively on the presence of localized electronic states that can trap charge and modify the local potentials near these interfaces [3–5]. In contrast to those of more conventional semiconductors such as Si and GaAs, the surface and interface properties of SiC are relatively unexplored.

As with other semiconductors, SiC of high electronic quality can be obtained from epitaxially grown films with thicknesses on the order of microns or less. In order to probe structures involving such films as well as their surfaces and interfaces, techniques are needed that have spatially confined excitation. Nanometre-scale localization represents a challenge for conventional optical and electrostatic techniques. Thus, for example, photoluminescence (PL) spectroscopy probes a volume defined by the absorption depth of light within the solid, typically fractions of a micron [6]. Likewise, deep-level transient spectroscopy (DLTS) and deep-level optical spectroscopy (DLOS) probe capacitance changes due to depletion width variations, typically on a hundred nanometre depth scale. On the other hand, surface-sensitive techniques such as photoemission spectroscopy and scanning probe techniques are hampered by their very nature in probing sub-surface electronic states, particularly near 'buried' interfaces, metal–semiconductor interfaces, or heterojunctions, for instance. Since localized states below surfaces or within sub-micron semiconductor films can influence charge transfer, carrier recombination, band bending, and band alignment, a technique is needed with near-surface sensitivity and variable depth capability on a nanometre scale.

One such technique is low-energy electron-excited nanoluminescence (LEEN) spectroscopy, a low-energy form of cathodoluminescence spectroscopy (CLS). This technique has provided new information on the energies, relative densities, and spatial distributions of localized electronic states for a wide variety of semiconductor surfaces, metal–semiconductor interfaces, and semiconductor–semiconductor heterojunctions (see, for example, [5], and references therein). A related technique is the higher-energy CLS with spatial localization defined by the electron excitation beam. Within the past few years, these techniques have revealed surprising new information when applied to SiC epitaxial layers. The combination of spatially localized excitation with optical spectroscopy can have unique advantages. When confined to surfaces and interfaces, optical spectroscopy can have much higher sensitivity to electronic states in the semiconductor band gap than other surface science techniques. Furthermore, considerable luminescence information is already available on electronic gap states of semiconductors. Extensive PL studies of SiC have established a multiplicity of band gap features due to impurities, point defects, morphological defects, and their complexes [7–9]. Such bulk information can be useful in identifying the physical nature of optical emissions observed at SiC surfaces and interfaces. Likewise, considerable information on SiC surface and metal contact properties is available from surface science techniques. See, for example, the excellent review by Bozack [10]. Here, we draw on such optical and surface science results in reviewing the electronic properties of SiC surfaces and interfaces measured by depth-resolved LEEN spectroscopy, CLS, and other electron-excited luminescence techniques.

2. Electron-excited luminescence spectroscopy

The electron-excited luminescence spectroscopy technique is based on the generation and recombination of free electron–hole pairs by an electron beam whose penetration and spatial extent are determined primarily by the energy and focal dimensions of the incident electron beam. For LEEN spectroscopy, incident beam energies E_B are only a few hundred to a few thousand volts. In this energy range, the electron cascade generated within the solid produces electron–hole pairs and optical emission that is localized from a few nanometres to a few hundred nanometres in depth, respectively [5, 11, 12]. Based on analytic expressions that depend on material density and incident energy, figure 1(a) illustrates plots of the electron–hole pair generation rate versus depth for SiC (inset), the depth U_0 at which this generation rate peaks, and the maximum range R_B of the electron cascade. For comparison, a Monte Carlo simulation of the electron cascade yields the graph shown in figure 1(b). Both figures illustrate

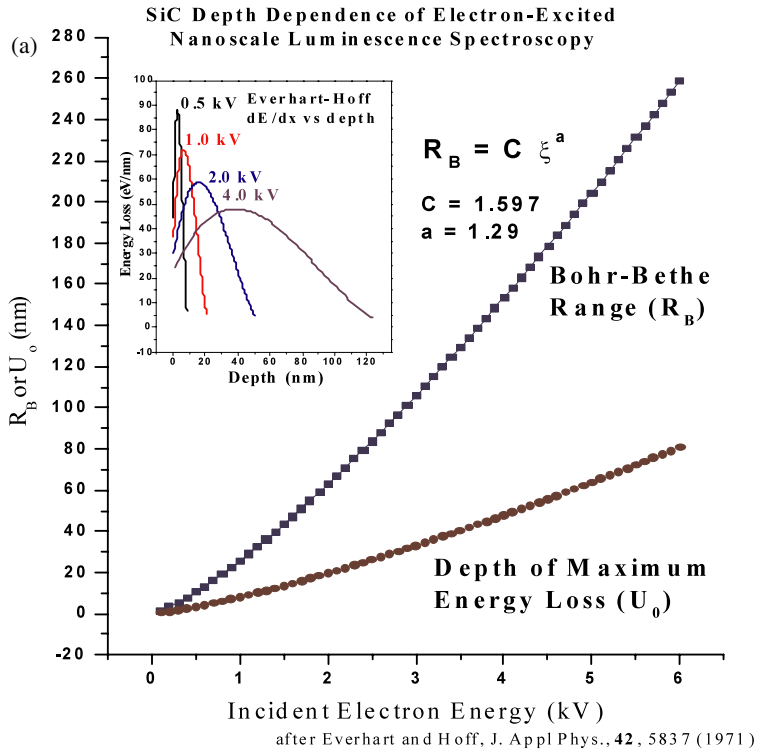

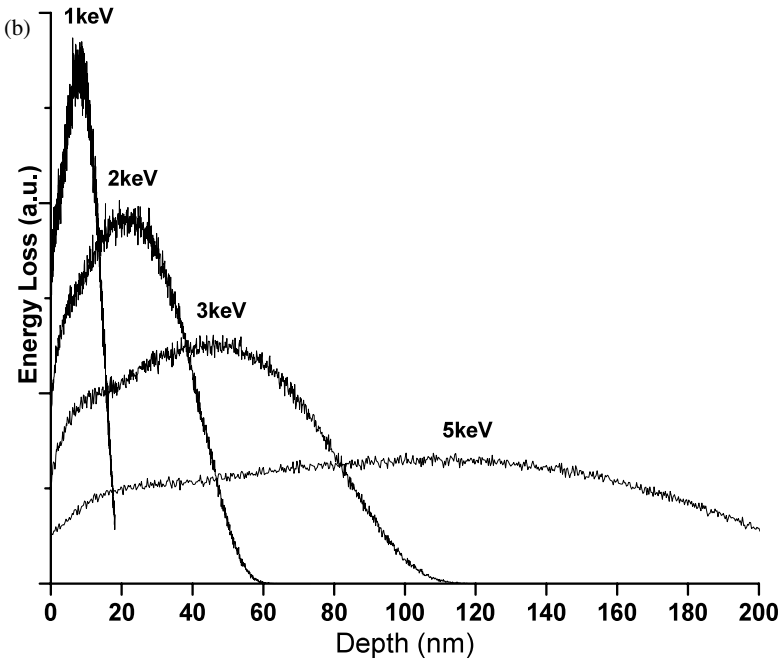

Figure 1. (a) The depth U_0 of the peak energy loss and the maximum depth R_B of the electron cascade [10, 11]. (b) Monte Carlo simulation of the electron–hole pair excitation rate versus depth in SiC, after [12].

the nanometre-scale depth range of relatively low-energy electrons in SiC. For $E_B < 1$ keV, excitation takes place primarily within a few nanometres of the free surface. For $E_B > 10$ keV, excitation can extend beyond a micron. While minority carrier diffusion defines the ultimate spatial resolution, such diffusion is relatively small near surfaces and interfaces, typically tens of nanometres or less [5]. States in the band gap act to reduce diffusion lengths dramatically, and such states are in fact the primary focus of electron-stimulated luminescence studies.

Electron-excited luminescence techniques are available using conventional ultrahigh-vacuum (UHV) surface science equipment. UHV not only enables the use of electron beams, but it also enables the atomic control of surfaces, while preventing the build-up of carbon contamination due to dissociation of residual gas by the electron beam. Such carbon layers not only alter the chemical nature of the surface, but also act as recombination sinks for free carriers that would otherwise recombine with optical emission. LEEN spectroscopy typically involves a low-energy electron gun such as that used for Auger electron spectroscopy (AES) and an optical collection system, typically a monochromator and photodetector. Variations on optical collection include glass lenses and windows, optical fibres, charge-coupled detectors, and metal optics. For higher-energy CLS, scanning electron microscope (SEM) columns enable spatially localized measurements of optical spectra and luminescence maps. Here again, UHV conditions are needed in order to probe surfaces susceptible to contamination.

3. Electronic states at and near SiC free surfaces

Surface science techniques have already provided considerable information on the properties of SiC surfaces. X-ray photoemission spectroscopy (XPS) and soft x-ray photoemission spectroscopy (SXPS) have yielded the valence band, band bending, and core level features of different SiC polytypes and orientations under a variety of surface conditions [10, 13, 14]. Scanning tunnelling microscopy (STM) has provided striking images of the various surface reconstructions that form under different thermal and adsorption treatments [15–17]. These studies have also identified several UHV procedures for obtaining clean, ordered surfaces, including annealing in a Si flux [18], high-temperature (1150 °C) annealing followed by subsequent Si deposition [19], flashing to 1250 °C [20], Si molecular beam etching at 900–1000 °C [21], and annealing under ethylene exposure [22]. These surface electronic and chemical analysis techniques have typical sensitivities at the 10^{13} cm^{-2}, i.e., 1% surface concentration, level. However, electronic states can affect electronic band bending and dipole formation significantly at charge densities that are orders of magnitude below such detection thresholds. Furthermore, it is important to distinguish electronic states near a surface or interface from those energy levels that are resident in the bulk material.

Figure 2 illustrates these capabilities for clean surfaces of 6H-SiC(0001) (Si face) and 6H-SiC(000$\bar{1}$) (C face) [23, 24]. Here the SiC specimens were single-side polished wafers initially cleaned *ex situ* by a trichloroethylene (TCE)/acetone/methanol degrease, a 2 min dip in 10:1 HF:H_2O, followed by a rinse in de-ionized (DI) H_2O. The specimens were blown dry and introduced into the UHV chamber. A thin SiO_2 layer together with small amounts of nitrogen and other adventitious elements remain after this treatment, as measured by AES. Annealing the specimen up to 500 °C removes the adventitious elements and most residual oxygen, leaving only a few per cent or less of residual O. Hence, the etch/anneal treatment removes most ambient contamination. All of the spectra in figure 2 are taken at 90 K. Dominating the spectral features is a peak centred at 0.92–0.95 eV, characteristic of V impurities in the SiC bulk crystal [25]. With decreasing E_B, excitation occurs closer to the free surface. Figure 2(a) shows that the 1.10 and 1.65 eV features increase relative to the 0.92 eV peak with surface excitation, indicating the surface nature of the 1.10 and 1.65 eV features and the surface sensitivity of the technique.

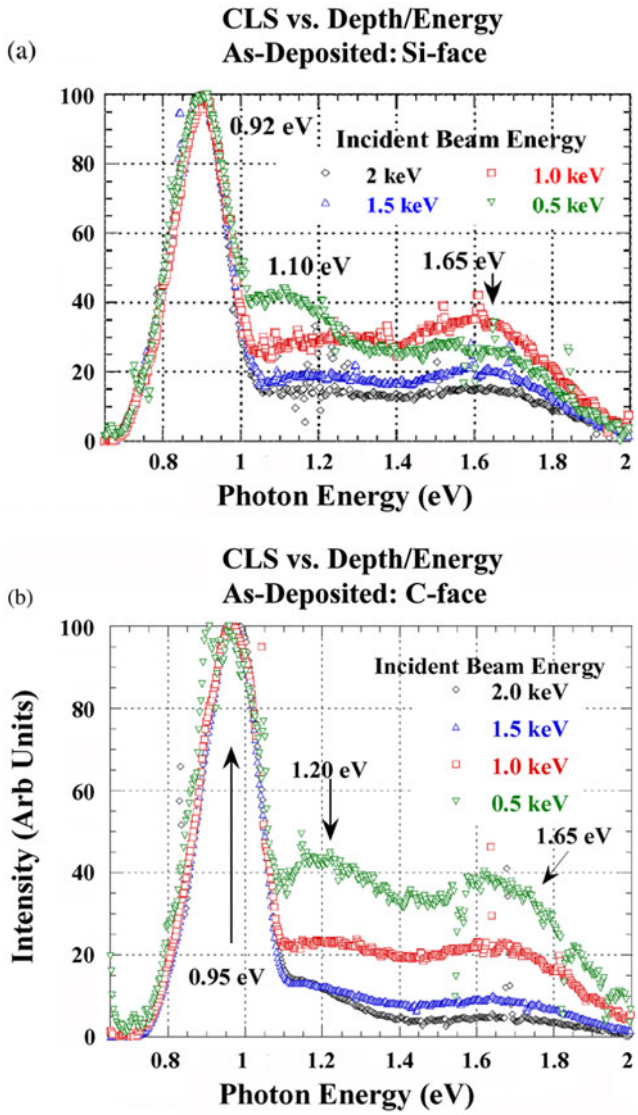

Figure 2. Depth-dependent CL spectra at 90 K of (a) Si face 6H-SiC and (b) as-cleaned C face. As E_B decreases, the peaks at 1.2 eV in (b) or 1.1 eV in (a) and 1.65 eV (both (a) and (b)) rise relative to the 0.92 eV V peak.

Figure 2(b) displays similar mid-gap luminescence features. Note, however, the clear difference in energy between the 1.10 eV peak for Si termination versus 1.20 eV for the C face. A 1.65 eV feature has been reported previously in optical detection of magnetic resonance (ODMR) experiments [26, 27] and attributed to a native defect whose atomic origin is as yet unknown. In 4H-SiC, a state located 1.10 eV above the valence band has been associated with intrinsic defects, specifically C vacancies, by photoinduced electron paramagnetic resonance (EPR) [28]. Here, annealing at 500 °C reduces the surface-related peaks at 1.10 and 1.20 eV and induces a new peak at 1.35 eV (not shown). Significantly, the 1.35 and the 1.65 eV peak energy sum to nearly the 3.03 eV band gap of bulk 6H-SiC. This suggests that these peaks are in fact complementary luminescence transitions from the same deep level rather than

chemically distinct defects. With continued annealing, LEEN spectra show a depletion of V within excitation depths of ∼10 nm and subsequent reintroduction of V from the bulk [24] at temperatures above the threshold for Si vacancy (and thereby impurity) diffusion [29]. Note that PL detection of these features and their changes with annealing would be impractical since the penetration depth of conventional laser excitation extends orders of magnitude beyond the near-surface region, e.g., 4.3 μm in 6H-SiC for 325 nm (He–Cd) photons [6]. Thus, free surface studies demonstrate that depth-resolved CLS or LEEN spectroscopy can detect and distinguish electronic states at, near, and below SiC surfaces that are due either to surface-localized states, bulk native defects, or impurities.

4. Process-dependent electronic states at metal–semiconductor interfaces

Electron-excited luminescence techniques can provide new information about the electronic properties of SiC interfaces with metals. Until recently, photoemission [30–34] and (most recently) ballistic energy electron (BEEM) [35] spectroscopies of SiC with only a few metal monolayers coverage have been the primary tools for examining electronic structure, measuring valence band densities of states, valence band thresholds, surface state emissions, or Fermi level positions within the band gap from which to infer interface state energies for SiC. Conventional electrical methods such as capacitance–voltage (C–V), current–voltage (I–V), and internal photoemission spectroscopy (IPS) have provided barrier heights at macroscopic metal overlayer thicknesses [36–42]. Electron-excited luminescence spectroscopy bridges these thickness regimes and is limited only by the attenuation of light through the metal overlayer—typically tens to hundreds of nanometres. Furthermore, the high sensitivity of optical techniques permits detection of signals from states with densities $<10^{15}$ cm^{-3}, comparable to transient capacitance probes [43, 44] and orders of magnitude lower than photoemission spectroscopies.

Figure 3 illustrates the sensitivity of depth-dependent electron-excited luminescence spectroscopy to electronic features near metal–SiC interfaces [45]. Shown here are results for a 6H-SiC interface with Pt/Ti, a metallization commonly used for ohmic contacts to SiC. These representative ohmic contact overlayers of Ti followed by Pt were thin enough to transmit significantly in the visible wavelength region, yet thick enough to manifest multilayer metallurgical behaviour. Pt/Ti/6H-SiC interfaces were formed by sputter deposition of 1–2 nm Ti followed by 2–3 nm Pt on chemically treated SiC samples, all from the same wafer and all in (0001) Si face orientation. The 6H-SiC wafers consisted of 2 μm thick, n-type ($N_d = 1.7\times10^{19}$ cm^{-3}) epilayers grown 8° off the basal (0001) plane on high-resistivity p-type substrates by chemical vapour deposition. Conventional processes for cleaning SiC samples consisted of the following sequential steps: (1) acetone and methanol cleaning, (2) dry oxidation at 1150 °C for 4 h to consume any SiC surface layer damage, (3) an HF strip and rinse with DI water to remove the oxidized SiC layer, and (4) a Piranha clean (1:1 volume ratio of H_2SO_4 and H_2O_2) to remove non-organic contamination. In figure 3(a), LEEN spectra of 6H-SiC cleaned using steps (1)–(3) are shown for E_B ranging from 1 to 4 keV, corresponding to U_0-depths ranging from 8 to 50 nm. For E_B lower than 1 keV they are relatively featureless since U_0 corresponds to excitation primarily in the 5 nm metal overlayer. The higher-energy spectra display the characteristic room temperature 6H-SiC polytype emission at 2.92–2.93 eV. With decreasing E_B, additional emissions are evident from the band edge down to energies of ∼1.5 eV, as well as at 3.3 eV. Figure 3(b) shows similar emissions and depth dependences of features with decreasing E_B for 6H-SiC cleaned using steps (1)–(4), including a Piranha clean. Indeed the continuum of emission below the band edge and a 3.3 eV emission are common to all the Pt/Ti/6H-SiC interfaces studied [45]. The sub-gap emissions are due to

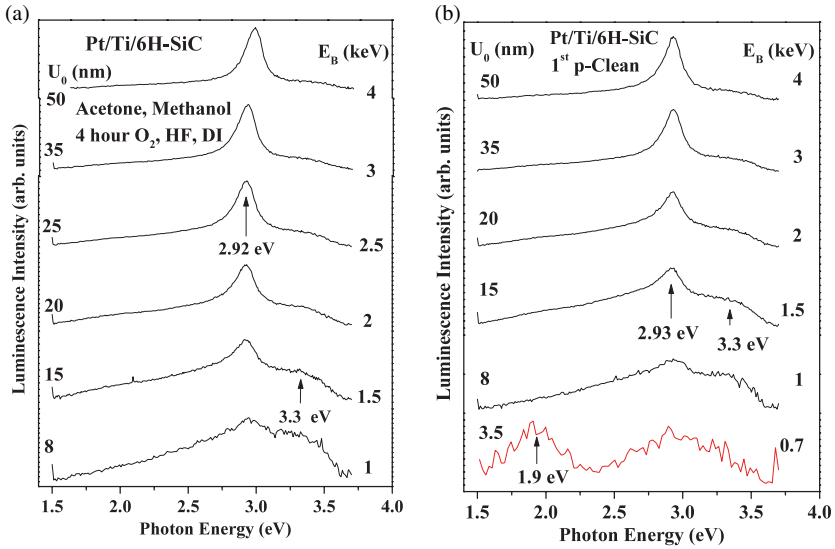

Figure 3. Depth-resolved 6H-SiC LEEN spectra after (a) acetone–methanol cleaning and metallization and (b) acetone–methanol cleaning, 4 h of dry oxidation, an HF oxide strip, a DI water rinse, and metallization. New phase formation is apparent near the interface in both cases.

transitions involving a continuum of states extending away from the 6H-SiC band edges. They are most pronounced at $E_B < 2$ keV, corresponding to the interface region ($U_0 < 15$ nm). The continuum of energies suggests that the localized states are due to defects with a multitude of lattice configurations/disorder. The intensity of the 3.3 eV feature exhibits a similar dependence on depth but resides at energies above the 6H-SiC band edge. Therefore it cannot be due to defect emission to or from states within the band gap. Rather it is attributed to broken 6H lattice periodicity and polytype variation near the interface. Based on its energy of 3.3–3.4 eV, this interfacial polytype variation appears similar to 2H-SiC, whose absorption edge resides at 3.33 eV [46]. This is the first demonstration of a SiC polytype change localized to an interface.

TEM micrographs confirm the altered nature of the Ti/6H-SiC interface. Figure 4 shows a TEM image for a 100 nm Ti film sputtered on a 6H-SiC epilayer independent of the samples described in figure 3. The image displays the sixfold periodicity of the 6H-SiC layer stacking in the bulk semiconductor (upper right). The crystal periodicity of the Ti metal can be seen as well to the left of the interface. Between these two regions, a layer appears that exhibits disruption of the 6H periodicity and possible formation of other polytypic phases. The thickness of this layer is ∼5 nm, in qualitative agreement with 10–15 nm depth of excitation beyond the initial 5 nm metal overlayer into the SiC over which the 3.3 eV and the continuum of states contribute significantly to the spectra in figure 3.

Figure 3(b) shows that the additional Piranha clean introduces an additional peak at 1.9 eV. This emission is evident only at the lowest incident beam energy and corresponds to the intimate Ti/SiC interface. Unlike the 2.9 eV, 3.3 eV, and continuum of gap states, this feature at 1.9 eV depends strongly on surface treatment before metallization. It appears initially after the first oxidation step and increases after Piranha cleaning. The subsequent reoxidation and oxide strip remove this feature and a second Piranha clean reintroduces it, albeit weakly. Atomic force microscopy (AFM) measurements showed that the sequence of cleaning steps (1)–(4) reduced the surface roughness substantially, from values of 0.6 to 0.3–0.4 nm, typically [47].

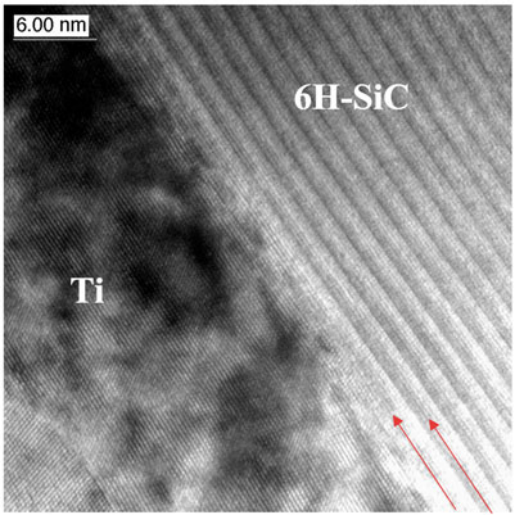

Figure 4. Cross-sectional TEM ($B = \langle 11\bar{2}0 \rangle$) of 100 nm Ti sputtered on 6H-SiC showing broken 6H periodicity in the interface region on a scale of ∼5 nm.

Hence, the 1.9 eV interface state in 6H-SiC does not appear to be related to surface roughness. The formation of this state is significant for at least two reasons—first, this interface state depends sensitively on the sequence of process steps and therefore on the local chemical composition and bonding; second, this state is nearly at mid-gap so, according to Shockley–Read–Hall statistics, it will promote strong recombination of charge carriers.

XPS analysis of the chemical bonding at the free SiC surface as a function of surface treatment reveals significant differences that reflect the changes in LEEN spectra [45, 47]. Monochromatized x-ray spectra of carbon 1s core levels prior to metallization exhibit a dominant peak corresponding to bulk SiC and a smaller shoulder corresponding to surface C with higher binding energy. The intensity of this shoulder decreases dramatically with the oxidation and HF strip, increases with the Piranha clean, decreases again with a second oxidation and HF strip, and remains low with a second Piranha clean. The intensity changes of this surface carbon shoulder mirror the intensity variation of the 1.9 eV LEEN feature, indicating the surface chemical nature of this electronic feature. Assuming that the C 1s shoulder is indicative of surface states, the reduction in this higher-binding-energy feature with oxidation is consistent with removal of adventitious C and any lattice damage.

Analogous measurements of 4H-SiC with Pt/Ti overlayers by electron-excited luminescence spectroscopy show a number of similarities. Figure 5 shows that, as with the Pt/Ti/6H-SiC specimens, the Pt/Ti/4H-SiC junction exhibits a pronounced continuum of states extending from the band edge to 1.5 eV. Similarly, emission above the band gap is again present—here again a broad shoulder at a slightly higher energy of 3.4 eV. The bulk excitation spectra ($E_B = 2$ keV) show the characteristic band edge feature of 4H-SiC at 3.2 eV. Both the continuum and the 3.4 eV emissions increase with proximity to the interface, again at a characteristic depth U_0 of 8–15 nm. As with the 6H interfaces, LEEN spectra at E_B corresponding to the interface show features that depend sensitively on surface treatment. In this case, a broad mid-gap peak appears at ∼2.0 eV after the oxidation/strip and increases with Piranha cleaning. Again, a second oxidation/strip reduces this feature. Also similar to the 6H-SiC spectra case, an additional Piranha cleaning does not reintroduce the near-mid-gap feature [47]. As with 6H-SiC, AFM and XPS studies show reduced surface roughness and adventitious carbon respectively with cleaning. In terms of near-surface chemical and interface state behaviour therefore, the 6H- and 4H-SiC exhibit similar behaviour.

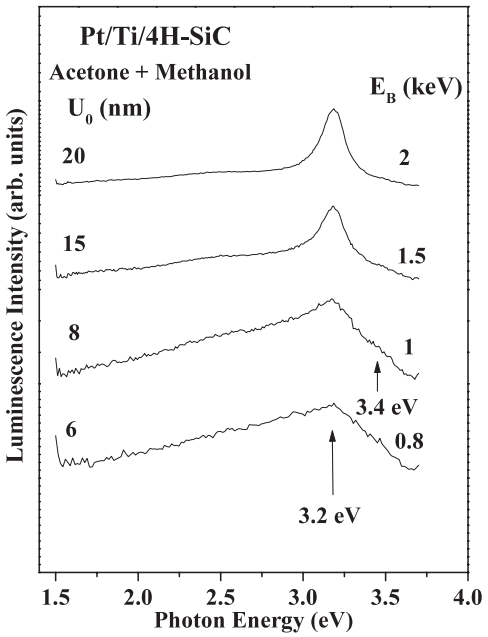

Figure 5. Depth-resolved LEEN spectra for 4H-SiC after an acetone/methanol clean and metallization.

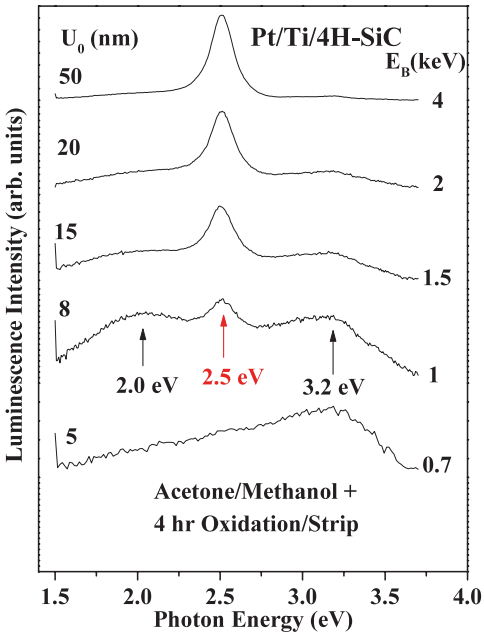

Figure 6. Depth-resolved 4H-SiC LEEN spectra after an acetone/methanol clean, a 4 h oxidation/HF strip, and metallization.

5. Polytype transformations

Notwithstanding their similarities, 4H-SiC and 6H-SiC display a striking difference in their morphological properties under mechanical or electrical stress. In terms of mechanical stress, Pirouz *et al* [48–50] showed that single-crystal SiC undergoes a polytype transformation when subjected to external mechanical loading. A polytypic transformation has also been reported for 4H-SiC during high-temperature etching with hydrogen [51] at 1575 °C and for 6H-SiC to 3C-SiC under vacuum conditions at 2080–2270 °C [52]. Lattice mismatch [53] and strain-induced stacking fault replication [54] are known to occur as a result of differences in doping between an epilayer and a 4H-SiC substrate.

5.1. Thermally induced polytype transformations

For heavily doped 4H-SiC epilayers, electron-excited luminescence spectroscopy shows that a polytype transformation can occur with thermal annealing at much lower temperatures—temperatures comparable to or less than those employed in the processing of SiC devices. Figure 6 illustrates the LEEN spectra for a 4H-SiC sample with $n = 1.7 \times 10^{19}$ cm^{-3} N doping after a methanol–acetone clean, a 4 h oxidation, and an HF strip, plus Pt/Ti metallization [55]. With the exception of the 4 h oxidation, the Pt/Ti/4H-SiC samples in figures 5 and 6 are identical. Figure 6 reveals the appearance of a pronounced new peak at 2.5 eV whose relative intensity increases with distance from the metal interface. The depth dependence of this feature indicates that it is not confined to the interface but rather extends into the 4H-SiC bulk crystal. It is not observed in any LEEN spectra of 6H-SiC under a wide array of thermal or chemical conditions [45]. Because the 2.5 eV peak linewidth is comparable to that of the bulk 4H-SiC

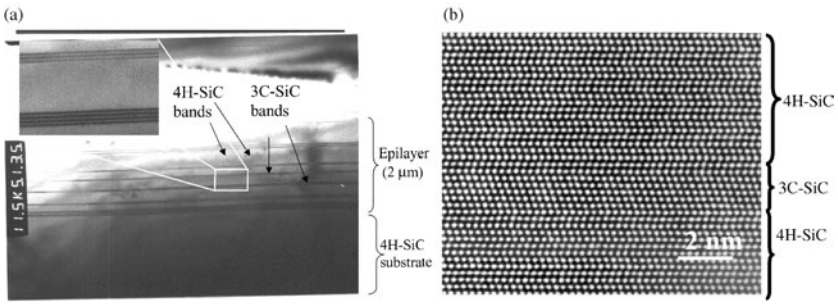

Figure 7. (a) The TEM cross-section after a 4 h oxidation at 1150 °C shows 3C planar bands interchanged with 4H-SiC bands. Each of the 3C bands is from two to several 3C unit cell heights thick; (b) HRTEM of the transformed 3C sub-band in 4H-SiC showing that one of the 3C-SiC sub-bands consists of seven Si–C bilayers.

near the band edge, this feature appears to be due to a new crystal polytype rather than point defects with a distribution of bonding arrangements.

TEM measurements confirm this morphological change and provide an explanation for the energy of this feature. Figure 7(a) shows a cross-sectional TEM image of a 4H-SiC epilayer on a 4H-SiC substrate after 1150 °C annealing for 4 h and without any metallization [45, 55]. An as-received, unoxidized 4H-SiC sample from the same $n = 1.7 \times 10^{19}$ cm^{-3} N-doped wafer shows no indication of polytypic transformation. However, after the thermal treatment, a striking morphological change occurs. The TEM lattice image reveals the presence of transformed crystalline regions that extend as planar 3C bands through the 4H-SiC crystal. These are believed to be the result of nucleation and propagation of $(1/3)\langle 10\bar{1}0\rangle$ Shockley partial dislocations on basal (0001) planes. Their nucleation may act to relieve the strain produced by the lattice mismatch between the heavily doped epilayer and the lightly doped substrate wafer [55]. Each of the 3C bands is from two to several 3C unit cell heights thick. The lowest thickness is most common and corresponds to a single stacking fault in the 4H-SiC lattice structure.

Figure 7(b) provides a closer view of a 3C band within the otherwise 4H-SiC lattice [56]. This 3C layer consists of seven Si–C bilayers and has a thickness equal to 1.75 nm. At such thicknesses, the conduction and valence band states of this 3C band can be described as quantum confined, so the NBE energy increases from its bulk 3C value. Comparing band offsets for 3C-SiC versus 6H-SiC [57] and 4H-SiC versus 6H-SiC [58], one can extract a cumulative 3C-SiC versus 4H-SiC conduction band offset value of $\Delta E_C = 0.84 \pm 0.1$ eV and a corresponding valence band offset ΔE_V of only 0.07 ± 0.1 eV. Thus the conduction band edge of the 3C-SiC lies lower in energy than that of the 4H-SiC, whereas the valence bands nearly align. In turn, this results in quantum confinement for electrons inside the 3C band but no confinement for holes. For a quantum well of width 1.5 nm, corresponding to two 3C unit cell repeat distances normal to the basal plane as shown in figure 7(b), the lowest-energy state for electrons with an effective mass $m_{\text{eff}} = 0.66\, m_0$ [59] is calculated to be 0.145 eV above the conduction band edge [45]. As a result, the bulk 3C-SiC NBE emission would increase within the transformation band from the reported band edge value of 2.39 (2.36 at room temperature) [60] to 2.5 eV. Hence the structural observations are in excellent agreement with the new optical feature discovered using electron-excited luminescence spectroscopy.

The transformation from the 4H-SiC to the 3C-SiC polytype induced by thermal oxidation can in fact take place under a variety of elevated temperature conditions. Annealing at 1150 °C

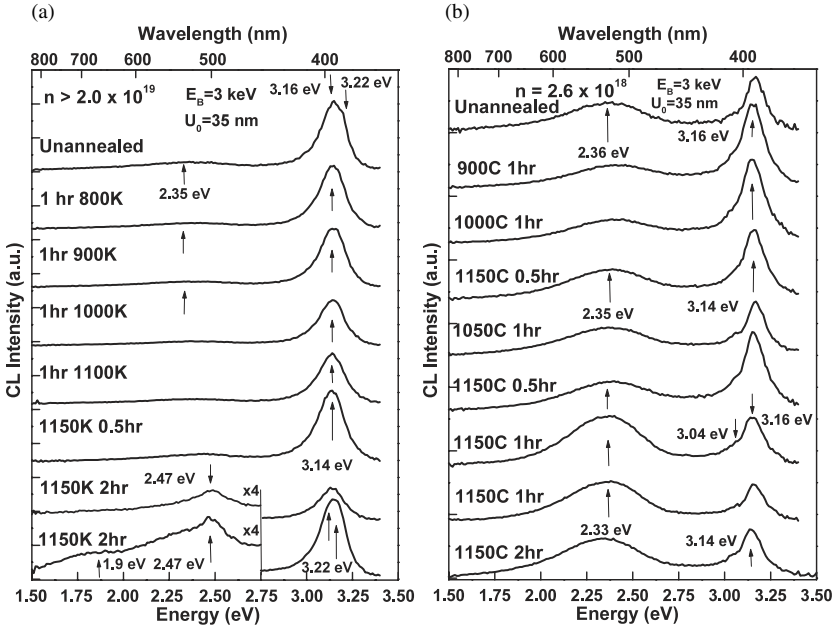

Figure 8. (a) 3 keV CL spectra of $>2.0 \times 10^{19}$ cm^{-3} 4H-SiC(0001) annealed in UHV. With increasing temperatures and times, new emissions appear at 2.47 and 1.9 eV; (b) 3 keV CL spectra of $>2.6 \times 10^{18}$ cm^{-3} 4H-SiC(0001) annealed in UHV. With increasing temperatures and times, no new emissions in the band gap appear.

in argon rather than oxygen also produces the 2.5 eV confined 3C emission in heavily doped 4H-SiC [55]. This 2.5 eV transformation peak also appears during annealing at 1150 °C in UHV [61]. Figure 8(a) illustrates the thermally induced changes in mid-gap optical emissions of an as-received 4H-SiC epilayer with doping $>2.0 \times 10^{19}$ cm^{-3}. The unannealed crystal exhibits a broad peak at 2.35 eV. At temperatures of 1150 °C for more than 0.5 h, the 2.5 eV feature appears. Continued annealing at this temperature leads to the appearance of a second, somewhat broader, feature at 1.9 eV. Significantly, these features are not present for 4H-SiC crystals with substantially lower doping. Figure 8(b) shows the annealing behaviour for 4H-SiC with 2.6×10^{18} cm^{-3} doping. Here, only the 2.35 eV broad emission is evident in the band gap at all temperatures. These observations show that a combination of temperature and doping rather than surface chemical conditions are important parameters governing the polytype transformation.

Electron-excited luminescence spectroscopy provides a tool for exploring the driving force for the change from the 4H-SiC to the 3C-SiC polytype. Factors that could play a role include: the strain due to differences in thermal expansion between the epilayer and substrate, injection of interstitials, creation of stacking faults, doping-induced differences in lattice constant, and electronic effects. Furthermore, these transformations can be deleterious to the performance of electronic devices, yet they occur at temperatures and doping levels often encountered in SiC microelectronic processing. If one understands the physical forces driving this structural change, one can identify process limits within which to control the structural changes.

Spectral measurements of the 3C-SiC feature versus temperature and time provide a means to obtain a thermal activation energy of the polytype transformation. Figure 9 illustrates CL spectra taken at 4 keV, corresponding to a peak excitation depth $U_0 = 50$ nm and characteristic

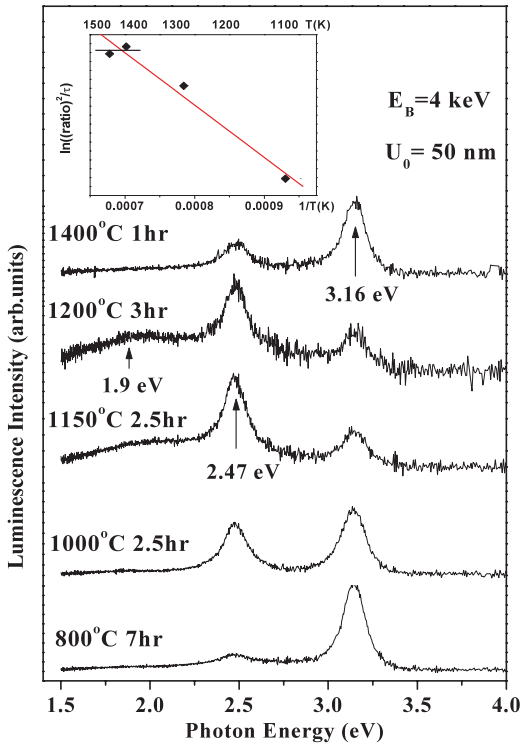

Figure 9. 4 keV CL spectra of different $n = 1.7 \times 10^{19}$ cm^{-3} 4H-SiC samples for various temperatures and times. The ∼2.5 eV peak appears at 800 °C and grows with temperature up to 1150 °C. The inset Arrhenius plot yields $E_A = 2.5 \pm 0.35$ eV.

of the subsurface region for 4H-SiC samples prepared by acetone/methanol cleaning and a 4 h oxidation/HF strip. Each spectrum corresponds to a different 4H-SiC specimen. All initial spectra exhibit the characteristic bulk 4H NBE emission at ∼3.2 eV. A 2.47 eV peak appears at the lowest thermal oxidation temperature of 800 °C after 7 h. After 2.5 h at 1000 °C, this peak is comparable in intensity to the 4H-SiC NBE emission. It increases further at 1150 °C after 2.5 h, reaching an intensity that is several times that of the bulk 4H-SiC NBE emission. At 1200 °C, little or no change occurs for a comparable anneal time. However, a broad 1.9 eV feature emerges in both 1150 and 1200 °C spectra, similar to the behaviour shown in figure 8(a). This suggests that an additional structural change takes place for highly doped 4H-SiC with high-temperature annealing. Significantly, these temperatures are well below the 1500–2000 °C temperatures typically employed for SiC epilayer growth and dopant activation [63]. At 1400 °C, the 2.47 eV peak decreases and the 3.16 eV 4H-SiC NBE peak increases, indicating that no additional structural changes occur in the 1200–1400 °C temperature range that contribute to further polytype transformation.

Besides temperature, a minimum anneal time is required to generate polytype transformation. Figure 10 illustrates the growth of the 2.47 eV feature with increasing anneal times at 1150 °C for samples otherwise identical to the 4H-SiC specimens used in figure 9. Again, each spectrum represents a separate 4H-SiC sample. The spectra show that a minimum anneal time of one hour is needed in order to induce the appearance of the 2.47 eV feature. By 1.5 h, this feature dominates the 4H-SiC NBE peak and remains so for

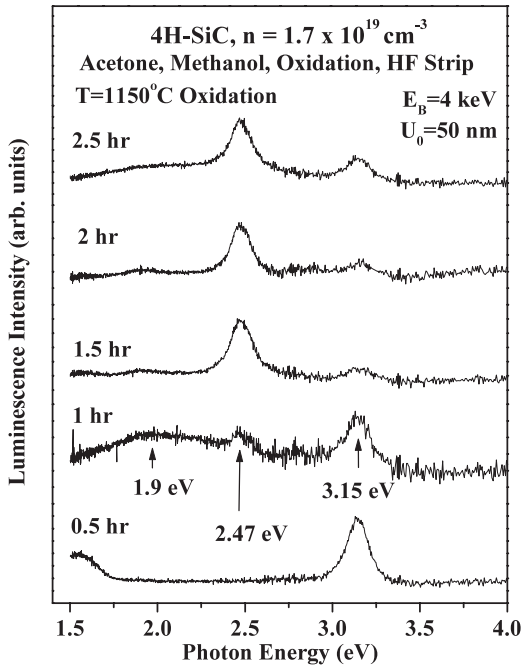

Figure 10. 4 keV CL spectra of different $n = 1.7 \times 10^{19}$ cm^{-3} 4H-SiC samples for a range of anneal times at 1150 °C. The 2.47 eV peak appears after 1 h.

additional annealing times. These temperature- and time-dependent results demonstrate that the polytype transformation is a thermally activated process. The intensities can be analysed using an Arrhenius plot, assuming that the emission intensities are proportional to the diffusion lengths $L = [D(T)t]^{1/2}$, where the diffusion constant $D(T) = D_0 e^{-E_A/kT}$ and D_0 is a constant. The figure 9 inset shows the Arrhenius plot of the time-normalized electron-excited luminescence peak intensity ratio $[I(2.5\text{ eV})/I(3.2\text{ eV})]^2/t$. It indicates an activation energy $E_A = 2.5 \pm 0.35$ eV for the 1.7×10^{19}cm^{-3} 4H-SiC. Significantly, this value is comparable to activation enthalpy changes for dislocation glide measured from mechanical deformation studies as a function of temperature at different fixed strain rates [64]. The existence of a thermal activation energy comparable to that measured for dislocation movement suggests that the 3C polytype transformation propagates via the bands observed with TEM from nucleation regions into the bulk of the 4H-SiC crystal.

The dependence on doping provides further insight into the physical mechanisms driving the cubic polytype transformation. Figure 11 illustrates 5 keV 'bulk'-like CL spectra for 4H-SiC after cleaning, 4 h 1150 °C oxidation, and HF stripping. Many of the spectra exhibit broad, sub-band gap features, particularly at 1.9 and 2.3–2.5 eV. However, only the 1.7×10^{19} cm^{-3} specimen displays a dominant 2.5 eV peak. Thus, only n-type 4H-SiC exhibits 3C-like features and only in the range of 4×10^{17}–1.7×10^{19} cm^{-3}. This behaviour indicates that high n-type doping is required for the transformation from the 4H-SiC to the 3C-SiC polytype.

This doping dependence can be interpreted in terms of the strain induced by the high concentration of N atoms substituting preferentially at carbon sites in the host lattice, which decreases the lattice constant relative to that of the substrate. Okojie *et al* [65] have confirmed this strain effect using high-resolution x-ray diffraction (HRXRD) to monitor the lattice constant of the epilayer as a function of doping and annealing. From the spatially averaged

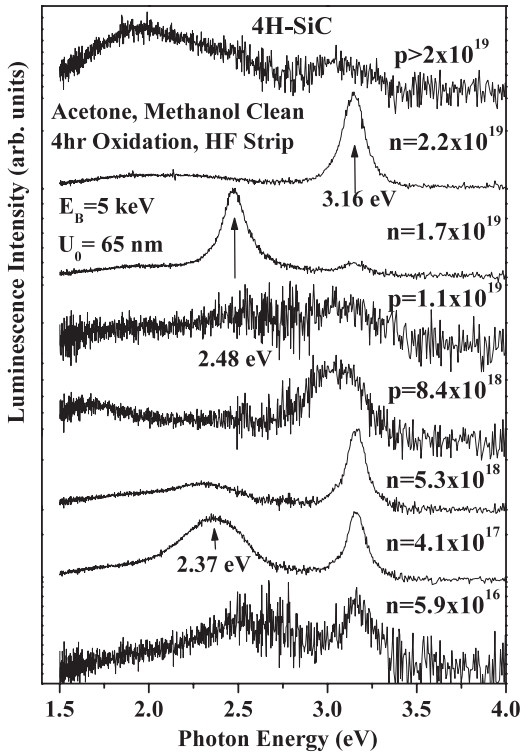

Figure 11. 5 keV CL spectra of cleaned and oxidized 4H-SiC as a function of doping concentration. Only $n = 1.7 \times 10^{19}$ cm^{-3} 4H-SiC exhibits a sharp peak at 2.48 eV.

lattice mismatch, determined from the rocking curve glancing incidence and glancing exit geometries, N doping of 4H-SiC increased the lattice strain about threefold for epilayers doped from 4.1×10^{17} to 1.7×10^{19} cm^{-3}. Furthermore, these HRXRD experiments showed a rapid decrease in strain for the 1.7×10^{19} cm^{-3} N after 1150 °C annealing and cooling to room temperature. Decreases in strain with annealing for less highly doped specimens were small or negligible. The decrease in strain with doping level after cooling from between 800 and 1150 °C suggests a relief mechanism via activation of mobile Shockley partials, resulting in a high density of stacking faults found only in the most highly doped epilayer [65]. Epilayers with even higher doping levels exhibited resolved multiple subsidiary peaks in the rocking curve that are likely to be due to a high density of low-angle grain boundaries rather than lattice mismatch or misorientation, suggesting a lower driving force for lattice relaxation. P-type doping with Al does not introduce large strain effects. Therefore, such p-type 4H-SiC is not expected to exhibit large strain effects, and strain-induced stacking fault generation is not expected.

5.2. Electronically driven polytype transformations

The formation of electronic states with lower energy than those in the bulk 4H-SiC represents another driving force for polytype transformation. In particular, Miao *et al* [66] and Iwata *et al* [67] have used first-principles calculations to show that stacking faults can introduce energy levels ∼0.2 eV below the conduction band edge of 4H-SiC. Therefore, stacking faults

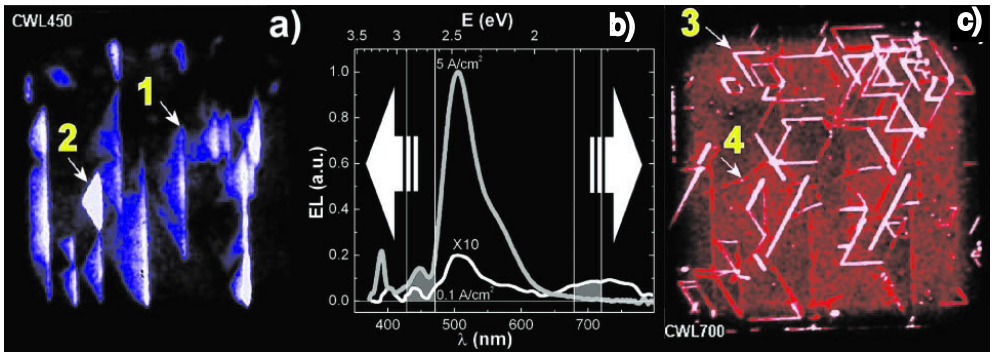

Figure 12. Plan-view electroluminescent images of an electrically degraded 4H-SiC p–i–n diode in wavelength ranges of 450 ± 20 nm (a) and 700 ± 20 nm (c). The full spectrum appears in (b). These spectrally filtered images indicate that light emission at 2.65–29 eV is associated with triangular stacking faults while emission at ∼1.8 eV is associated with dislocations bordering these triangular faults (after [73], with permission).

should be energetically favourable in highly n-type 4H-SiC because the Fermi level would then be above the stacking fault level, providing a lower energy for electrons than the 4H-SiC conduction band. Significantly, the Fermi level at the 1150 °C annealing temperatures is above this 0.2 eV level only for doping levels in excess of $\sim 10^{19}$ cm^{-3}. At lower doping levels, the Fermi level drops toward the middle of the band gap at high temperatures due to intrinsic carrier generation [62, 68]. In this regard, the decrease in 2.47 eV versus 4H-SiC NBE emission at 1400 °C in figure 9 can be interpreted as Fermi level lowering below the stacking fault level with increased temperature, consistent with the Lambrecht model [62]. This model is also consistent with the absence of 2.47 eV emission in p-type 4H-SiC since the Fermi level is always below the proposed stacking fault level. Kuhr *et al* [69] have presented a quantitative analysis of this electronic mechanism of stacking fault generation and confirm that doping levels in excess of $\sim 10^{19}$ cm^{-3} raise the Fermi level above a level E_C (4H-SiC)–0.2 eV.

5.3. Electrically stressed polytype transformations

Other luminescence spectroscopy measurements can provide further insight into these mechanisms. The application of forward voltage to 4H-SiC p–n diodes over extended time periods leads to the creation of structural defects in the epitaxial layers [70]. Low-temperature panchromatic CL images of such electrically stressed 4H-SiC diodes reveal triangular and rectangular features with reduced emission on stressed versus unstressed diodes. These darker regions were interpreted as stacking faults that propagate in the basal plane. Stahlbush and MacFarlane [71] observed the time-dependent movement of these 3C inclusions, identified from their 2.3 eV peak energy, in electrically stressed SiC metal–oxide–semiconductor field effect transistors (MOSFETs). They also analysed the emission spectrally, finding a broad emission from 1.5–2.5 eV that they attributed mainly to interface traps. This mid-gap emission appeared much more pronounced in spectra of 4H- versus 6H-SiC MOSFETs.

Galeckas *et al* performed optical emission microscopy on electrically stressed 4H-SiC p–i–n diodes [72, 73] and showed that built-in defects can act as nucleation sites for stacking faults. In addition, they directly measured the dislocation velocity as a function of the absolute temperature from recordings of dislocation motion at constant injection current density [73]. In figure 12, their spectrally filtered images at room temperature show ∼2.8 eV luminescence

across the entire triangular stacking area, consistent with the predictions by Lindefelt *et al* [67] and Miao *et al* [66] of a quasi-two-dimensional band of energies split off from the 4H-SiC conduction band by ∼0.2 eV. Significantly, emissions in this range are not apparent in the spectra illustrated in figures 6 and 8. This suggests a difference in the electronic states produced by electrical versus thermal stress. Galeckas *et al* [73] also found significant emission at ∼1.8 eV that appeared localized at partial dislocations bordering the stacking faults as well as at screw and/or edge threading dislocations; see figure 12. This observation is similar to the appearance of a broad emission feature around 1.9–2 eV in figures 6 and 8 with annealing and stacking fault formation. Hence, the identification of the 1.9–2 eV feature with partial, screw, and/or edge threading dislocations is consistent with both thermally and electrically driven experiments. Galeckas *et al* [73] also found strong emission at 2.43 eV with a shoulder at ∼2.3 eV, which they attributed to boron impurities based on previous studies of B-doped 4H-SiC [74]. The measurements of dislocation motion lead to an activation energy of 0.27 ± 0.02 eV. Since an activation energy of ∼2.5 eV is estimated for dislocation glide in 4H-SiC [64], they concluded that the reduction in dislocation glide energy of ∼2.2 eV is due to non-radiative recombination that redirects the energy into the crystal lattice. Such a non-radiative recombination mechanism is believed to promote defect reactions in semiconductors [75, 76].

Recently, Skromme *et al* [77, 78] and Zimmerman *et al* [79] have also observed transformed lamellae using just an SEM in the secondary-electron image mode. The ability to detect to visualize the intersection of such lamellae with the vicinal surface is attributed to charge contrast arising from transfer of electrons from the 4H host matrix to the quantum well regions within the lamellae. The SEM images show a high density of stacking faults in a heavily doped n-type SiC substrate that terminate at the interface with a lightly doped SiC epitaxial layer [77, 79]. This result argues against a stress mechanism driven by doping-induced lattice mismatch since such stress should reside within the epilayer rather than in the substrate. On the other hand, Okojie *et al* [55] found transformation bands of stacking faults confined to heavily n-type 4H-SiC epilayers on more lightly doped SiC substrates—in support of a stress-induced mechanism. Liu *et al* [80] analysed stacking sequences and partial dislocations bounding the stacking faults in electrically stressed diodes and suggested that the stress driving their fault formation is local in origin. Overall, electron-excited luminescence and microstructural results favour an electronic mechanism, although evidence exists for mechanical stress relaxation with polytype transformation. Both mechanisms may in fact play a role since there appear to be significant spectral differences between 4H-SiC transformed under thermally versus electrically induced stress.

6. Correlations with PL spectroscopy

PL spectroscopy measurements complement the electron-excited luminescence results and help explain additional 4H-SiC mid-gap features. The low-temperature PL spectroscopy of Skromme *et al* [81] confirms the effect of high-temperature annealing on highly n-type 4H-SiC. They observe the appearance of a series of sharp peaks in the range of 2.4–2.5 eV for wafers oxidized at 1150 °C for 90 min which they attributed to 3C formation as well. Temperature-dependent PL measurements of 4H-SiC with different doping concentrations and thermal treatments show a broad ∼2.4 eV feature similar to that evident in figures 8, 9, and 11 [82]. This peak appears at temperatures above ∼85 °C and dominates all other features for temperatures up to ∼200 °C. Significantly, it is present in all 4H-SiC specimens, regardless of doping or thermal treatment. The energy and temperature dependence of this PL feature is similar to that reported previously in B-doped 4H-SiC studies and is not unexpected, given the use of B in crystal growth facilities [74, 83, 84]. Such B impurities may well account for the 2.35 eV

emission evident in figures 8(a) and (b). On the other hand, this broad ∼2.4 eV peak could also be viewed in terms of 3C inclusions in the 4H-SiC host crystal. Such inclusions are known to be present in SiC and nucleate preferentially during growth of 4H versus 6H material [85, 86]. Bulk 3C-SiC NBE emission is below 2.39 eV. But for small enough inclusions, this energy will be higher due to quantum confinement. Furthermore, if these inclusions have variable size, they will exhibit a broad range of energies. Approximating such inclusions as platelets whose layer thickness defines the maximum emission energy, one obtains a range of sizes from 1.5 to 5 nm that can account for the range of energies contained within the ∼2.4 eV shoulder [82]. The presence of such 3C inclusions in 4H-SiC could provide the nucleation sites from which the transformation bands propagate. Other PL research relates emissions in the range of 2.9–3 eV to electrically induced stacking fault formation [87, 88]. These results are notable since there is no detectable emission at 2.9 eV in the LEEN spectra of figures 6, 9, 10, or 11, despite the appearance of the 2.5 eV 3C feature. The 2.9 eV feature seen in electrically stressed 4H-SiC is consistent with the prediction of a localized state 0.2–0.3 eV below the 4H-SiC band edge [66, 67]. On the other hand, *ab initio* calculations predict that deeper states can form with increase in the number of neighbouring stacking faults. These bound states have energies of 0.55, 0.65, and 0.75 eV for two, three, or four neighbouring stacking faults, respectively [89]. Referenced with respect to the 4H-SiC valence band, these states would then lie at energies around 2.45–2.65 eV, near the quantum-confined 3C-SiC band gap energy and the thermally induced 2.5 eV peak shown above. The absence of the 2.9 eV emission in the thermally stressed, highly n-type 4H-SiC suggests that different localized states may be induced by thermal versus electrical stress.

7. Schottky barrier effects

The electron-excited luminescence studies of SiC surfaces and interfaces provide evidence for localized states that could influence charge transfer at metal–SiC junctions. Until now, such states were only inferred, on the basis of the variations in Fermi level position with metal work function, rather than measured directly. Figures 2, 3, 5, and 6 show that surface states are present at energies across the 6H- and 4H-SiC band gap. The variable nature of these states with different chemical treatments and near-interface lattice structure indicates their sensitivity to local chemical bonding. By the same token, no gap state emission is evident that is common to all or dominates all other emission in these spectra. This fact is consistent with the reported lack of strong Fermi level stabilization at a high density of states, i.e., 'pinning', at metal/4H-SiC or metal/6H-SiC interfaces. Schottky barrier studies performed on 4H-, 6H-, and 3C-SiC with a wide range of metals show no strong Fermi level pinning for all polytypes. Instead, the Schottky barrier heights exhibit linear relationships with the metal work function with slopes of ∼0.2–0.7 eV [36, 38]. On this basis, localized states appear to exert only a moderate influence on the Fermi level position in the SiC band gap.

One likely candidate for producing such 'pinning' effects is the 1.9 eV feature in figure 3 measured with a visible/UV detector and induced by chemical treatment in 6H-SiC followed by Ti and Pt deposition. For the 2.93 eV 6H-SiC energy gap, the band gap complement of this emission energy equals 1.03 eV. This is close to the 1.1 eV emission shown in figure 2(a) measured with a near-infrared detector for the Si face of 6H-SiC. These complementary transition energies indicate states either 1.9 eV above the valence band or 1.9 eV below the conduction band. States located 1.03 eV below the conduction band are close to the Schottky barrier of 0.93–0.97 eV for Ti on the Si face of 6H-SiC after a 30 s, 400 °C anneal (to promote a more reacted, intimate contact) [30] as well as the Si-face Schottky barrier for Pt of 1.06 eV for as-deposited metal [36]. It is also significant that the 1.1 eV peak for the Si face in figure 2(a)

shifts to 1.2 eV in the C-face spectra shown in figure 2(b). This agrees with the 0.1–0.2 eV increase in Schottky barrier height for C-face versus Si-face barrier heights measured for Ti/6H-SiC contacts as well as a similar trend for metal–SiC interfaces in general [38]. Similar analysis for the complement of 1.35 and 1.65 eV peaks found after a 500 °C anneal suggests states somewhat deeper within the 6H-SiC band gap. Significantly, neither set of states are high enough in density to 'pin' the n-type 6H-SiC Fermi level in a narrow energy range. Indeed, for unreactive metals [2] on the less reactive Si face, barrier heights can range up to 1.4 eV [90]. While a broad continuum of states is present very close to the metal interface, its relative emission intensity is less than that of the discrete states, suggesting that its influence on Fermi level movements is even less important. The significant changes reported for SiC specimens for the same metal with different process treatments are in accordance with the creation of different gap states depending on local chemical bonding and diffusion.

Schottky barrier variations are evident across SiC wafer surfaces and from wafer to wafer, depending on local chemical or morphological changes. Electron beam-induced current (EBIC) imaging reveals dark patches attributed to recombination centres and discrete crystal defects that correlate with localized low-barrier-height patches and ideality factors greater than one [42]. Likewise, reactive ion etching produces strong Fermi level 'pinning' on 4H-SiC, i.e., similar barrier heights for metals of quite different work functions [41]. In effect, the CHF_3/O_2 etching introduces either an increased interfacial layer or near-surface defects that reduce the Fermi level movement for metals with different work function. Both results demonstrate the importance of surface defects for the electronic properties of metal–SiC interfaces. Skromme *et al* [81] have also shown that Schottky barriers for Pt, Ni, and Ti are uniformly lower by 0.4–0.5 eV for different areas of highly n-doped ($>1 \times 10^{19}$ cm^{-3} N) 4H-SiC bulk wafers after high-temperature (1150 °C for 90 min) oxidation. Since these metals have very different work functions, a natural explanation for the systematically different barrier heights is the presence of transformed SiC regions with 0.4–0.5 eV higher electron affinity in the lower-barrier-height regions. Such higher electron affinity follows the 0.84 eV deeper conduction band inferred from the 3C- versus 4H-SiC band offset calculations and suggests that the measured Schottky barrier differences reflect two different polytypes. Here again, variations across the SiC surface manifest themselves in electronic transport measurements.

8. Future surface and interface studies

The electron-excited luminescence spectroscopy results presented here show that localized electronic states are present at SiC surfaces and interfaces, and that they are sensitive to chemical treatments and lattice transformations. Certainly, the combination of high n-type doping and high temperature has dramatic effects on both structural and electronic properties of the metal/4H-SiC interface. In addition to oxidation and contact annealing during device fabrication, metal–SiC junctions must also function electronically at high temperatures. Thus, studies are needed to probe the interdiffusion of metals with SiC at elevated temperatures in UHV. Such interdiffusion can promote the formation of native defects, e.g., Si and C vacancies and their complexes, as well as metal impurity states in the SiC. LEEN spectroscopy can probe the electronic states formed as a function of temperature and depth from the intimate contact on a nanometre scale. Cross-sectional CLS and TEM measurements as well as micro-SIMS can provide complementary electronic, structural, and chemical information on a microscopic scale. Among the issues that this combination of measurements can address are: What are the energies of localized states produced at the annealed metal/4H-SiC or 6H-SiC interface? Do native point defects, metal impurity states, or morphological defects dominate these local electronic features? How does the chemical reactivity of the metal/SiC interface affect the

interdiffusion process? What effects do the local polytype changes at the SiC interface have on Schottky barriers for metals in general? How do high levels of n- or p-type doping affect the formation of these localized states? What are the diffusion coefficients for native defect or impurity diffusion and the corresponding time/temperature thresholds for electronic stability? While many of these questions can be directed toward ensuring the electronic stability of these SiC interface structures, this information could in principle be used to identify process conditions for creating new heterojunction structures with unique electronic properties.

9. Conclusions

Silicon carbide surfaces and interfaces provide a remarkable array of electronic and structural features that depend sensitively on chemical and thermal treatment. These features can have major effects on basic measurements as well as the variety of applications envisioned for this material. Electron-excited luminescence measurements have already begun to reveal some of the systematic connections between morphological and electronic structure. With the advent of spatially localized CLS and LEEN spectroscopy in an electron microscope, a new avenue is available for associating the local electronic states of SiC with its microscopic structural properties.

Acknowledgments

This work was supported by the National Aeronautics and Space Administration under the Glennan Microsystems Initiative with additional support from the Office of Naval Research, the Department of Energy, and the National Science Foundation.

References

[1] Morkoc H, Strite S, Gao G B, Lin M E, Sverdlov B and Burns M 1994 Large-band-gap SiC, III–V nitride, and II–VI ZnSe-based semiconductor device technologies *J. Appl. Phys.* **76** 1363

[2] Brillson L J 1989 Metal semiconductor contacts: electronic structure of the interface *Comment. Condens. Matter. Phys.* **14** 311

[3] Brillson L J 1982 The structure and properties of metal–semiconductor interfaces *Surf. Sci. Rep.* **2** 123

[4] Brillson L J 1992 Surfaces and interfaces: atomic-scale structure, band bending and band offsets *Handbook on Semiconductors* vol 1, ed P T Landsberg (Amsterdam: North-Holland) chapter 7, pp 281–417

[5] Brillson L J 2001 Nanoscale luminescence spectroscopy of defects at buried interfaces and ultra-thin films *J. Vac. Sci. Technol.* B **19** 1762

[6] Sridhara S G, Eperjesi T J, Devaty R P and Choyke W J 1999 Penetration depths in the ultraviolet for 4H, 6H, and 3C silicon carbide at seven common laser pumping wavelengths *Mater. Sci. Eng.* B **61** 229

[7] Devaty R P and Choyke W J 1997 Optical characterization of silicon carbide polytypes *Phys. Status Solidi* a **162** 5

[8] Schneider J and Maier K 1993 Point defects in silicon carbide *Physica* B **185** 199

[9] Sridhara S G, Carlsson F H C, Bergman J P and Janzén E 2001 Luminescence from stacking faults in 4H-SiC *Appl. Phys. Lett.* **79** 3944

[10] Bozack M J 1997 Surface studies on SiC as related to contacts *Phys. Status Solidi* b **202** 549

[11] Everhart T E and Hoff P H 1971 *J. Appl. Phys.* **42** 5837
Kanaya K and Okayama S 1972 *J. Phys. D: Appl. Phys.* **5** 43
Shea S P 1984 *Electron Beam Interactions with Solids* ed D F Kyser, D E Newbury, H Niedrig and R Shimizu (Chicago: SEM) pp 145–51

[12] Hovington P, Drouin D and Gauvin R 1997 CASINO: a new Monte Carlo code in C language for electron beam interaction—part I: description of the program *Scanning* **19** 1 (http://www.gel.usherb.ca/casino/)

[13] Bermudez V M and Long J P 1995 Characterization of reconstructed SiC(100) surfaces using soft x-ray photoemission spectroscopy *Appl. Phys. Lett.* **66** 475

[14] Hüsken H, Schroter B and Richter Wo 1998 Surface state dispersion on the β-SiC(111)-(3 $\times$ 3) surface *Surf. Sci.* **407** L676
[15] Semond F, Soukiassian P, Mayne A, Dujardin G, Douillard L and Jaussard C 1996 Atomic structure of the beta-SiC(100)-(3 $\times$ 2) surface *Phys. Rev. Lett.* **77** 2013
[16] Soukiassian P, Semond F, Douillard L, Mayne A, Dujardin G, Pizzagalli L and Joachim C 1997 Direct observation of a beta-SiC(100)-c(4 $\times$ 2) surface reconstruction *Phys. Rev. Lett.* **78** 907
[17] Owman F and Martensson P 1996 Scanning tunnelling microscopy study of SiC(0001) surface reconstructions *J. Vac. Sci. Technol.* B **14** 933
[18] Bermudez V M 1992 Study of the initial adsorption of nitrogen on SiC(100)-(2 $\times$ 1) *Surf. Sci.* **276** 59
[19] Semond F, Douillard L, Soukiassian P, Dunham D, Amy F and Rivillon S 1996 Direct SiO_2/beta-SiC(100)3 $\times$ 2 interface formation from 25 °C to 500 °C *Appl. Phys. Lett.* **68** 2144
[20] Bermudez V M 1989 Photoemission study of oxygen adsorption on (001) silicon carbide surfaces *J. Appl. Phys.* **66** 6084
[21] Li L, Hasegawa Y and Sakurai T 1997 Si- and C-rich structure of the 6H-SiC(0001) surface *J. Vac. Sci. Technol.* B **15** 1307
[22] Bermudez V M and Kaplan R 1991 Preparation and characterization of carbon-terminated beta-SiC(001) surfaces *Phys. Rev.* B **44** 11149
[23] Young A P, Jones J and Brillson L J 1999 Low energy cathodoluminescence spectroscopy of etched 6H-SiC *J. Vac. Sci. Technol.* A **17** 2692
[24] Young A P, Aptowitz K and Brillson L J 1998 Cathodoluminescence deep level spectroscopy of etched and *in situ* annealed 6H-SiC *Mater. Res. Soc. Proc.* **525** 151
[25] Schneider J, Muller H D, Maier K, Wilkening W and Fuchs F 1990 Infrared spectra and electron spin resonance of vanadium deep level impurities in silicon carbide *Appl. Phys. Lett.* **56** 1184
[26] Janzén E, Kordina O, Henry A, Chen W M, Son N T, Monemar B, Sörman E, Bergman P, Harris C I, Yakimova R, Tuominen M, Konstantinov A O, Hallin C and Hemmingsson C C 1994 SiC—a semiconductor for high-power, high-temperature and high-frequency devices *Phys. Scr.* T **54** 283
[27] Son N T, Sörman E, Chen W M, Kordina O, Monemar B and Janzén E 1994 Possible lifetime-limiting defect in 6H-SiC *Appl. Phys. Lett.* **65** 2687
[28] Dvanut M E and Konovalov V V 2002 The level position of a deep intrinsic defect in 4H-SiC studied by photoinduced electron paramagnetic resonance *Appl. Phys. Lett.* **80** 410
[29] Itoh H, Hayakawa N, Nashiyama I and Sakuma E 1989 Electron spin resonance in electron-irradiated 3C-SiC *J. Appl. Phys.* **66** 4529
[30] Waldrop J R and Grant R W 1993 Schottky barrier height and interface chemistry of annealed metal contacts to alpha 6H-SiC: crystal face dependence *Appl. Phys. Lett.* **62** 2685
[31] Waldrop J R and Grant R W 1990 Formation and Schottky barrier height of metal contacts to beta-SiC *Appl. Phys. Lett.* **56** 557
[32] Waldrop J R, Grant R W, Wang Y C and Davis R F 1992 Metal Schottky barrier contacts to alpha 6H-SiC *Appl. Phys. Lett.* **72** 4757
[33] Van Elsbergen V, Kampen T U and Monch W 1996 Electronic properties of cesium on 6H-SiC surfaces *J. Appl. Phys.* **79** 316
[34] Virojanadara C, Glans P-A, Balasubramanian T, Johansson Li I, Macak E B, Wahab Q and Madsen L D 2002 Schottky barrier height studies of Au/4H-SiC(0001) using photoemission and synchrotron radiation *J. Electron. Mater.* **31** 1353
[35] Im H-J, Kaczer B, Pelz J P and Choyke W J 1998 Ballistic electron emission microscopy of Schottky contacts *Appl. Phys. Lett.* **72** 839
[36] Porter L M and Davis R F 1995 A critical review of ohmic and rectifying contacts for silicon carbide *Mater. Sci. Eng.* B **34** 83
[37] Syrkin A L, Andreev A N, Lebedev A A, Rastegaeva M G and Chelnokov V E 1995 Metal–n-6H-SiC surface barrier height—experimental data and description in the traditional terms *J. Appl. Phys.* **78** 5511
[38] Itoh A and Matsunami H 1997 Analysis of Schottky barrier heights of metal/SiC contacts and its possible application to high-voltage rectifying devices *Phys. Status Solidi* a **162** 389
[39] Lee S-K, Zetterling C-M and Ostling M 2000 Schottky diode formation and characterization of titanium tungsten to n- and p-type 4H silicon carbide *J. Appl. Phys.* **87** 8039
[40] Raynaud C, Isoird K, Lazar M, Johnson C M and Wright N 2002 Barrier height determination of SiC Schottky diodes by capacitance and current–voltage measurements *J. Appl. Phys.* **91** 9841
[41] Skromme B J, Luckowski E, Moore K, Clemens S, Resnick D, Gehoski T and Ganser D 2000 Fermi level pinning and Schottky barrier characteristics on reactively ion etched 4H-SiC *Mater. Sci. Forum* **338–342** 1029

[42] Skromme B J, Luckowski E, Moore K, Bhatnagar M, Weitzel C E, Gehoski T and Ganser D 2000 Electrical characteristics of Schottky barriers on 4H-SiC: the effects of barrier height nonuniformity *J. Electron. Mater.* **29** 376
[43] Hierro A, Kwon D, Goss S H, Brillson L J and Ringel S A 1999 Evidence for a dominant mid-gap trap in n-ZnSe grown by molecular beam epitaxy *Appl. Phys. Lett.* **75** 832
[44] Hierro A, Kwon D, Ringel S A, Brillson L J, Schaefer J, Young A P and Franciosi A 1999 Deep level characterization of interface-engineered ZnSe layers on GaAs grown by molecular beam epitaxy *MRS Proc.* vol 535 (Warrendale, PA: Materials Research Society) p 99
[45] Tumakha S, Brillson L J, Jessen G H, Okojie R S, Lukco D, Zhang M and Pirouz P 2002 Chemically dependent traps and polytypes at Pt/Ti contacts to 4H and 6H-SiC *J. Vac. Sci. Technol.* B **20** 554
[46] Patrick L, Hamilton D R and Choyke W J 1966 Growth, luminescence, selection rules, and lattice sums of SiC with wurtzite structure *Phys. Rev.* **143** 526
[47] Okojie R S, Lukco D, Keys L, Tumakha S and Brillson L J 2002 Surface morphology and chemistry of 4H- and 6H-SiC after cyclic oxidation *Mater. Sci. Forum* **389–393** 1101
[48] Yang J W and Pirouz P 1993 The $\alpha \rightarrow \beta$ polytypic transformation in high-temperature indented SiC *J. Mater. Res.* **8** 2902
[49] Pirouz P and Yang J W 1993 Polytypic transformations in SiC: the role of TEM *Ultramicroscopy* **51** 189
[50] Hong M H, Samant A V and Pirouz P 2000 Stacking fault energy of 6H-SiC and 4H-SiC single crystals *Phil. Mag.* A **80** 919
[51] Powell J A, Larkin D J and Trunek A J 1998 Gaseous etching for characterization of structural defects in silicon carbide single crystals *Mater. Sci. Forum* **264** 421
[52] Vlaskina S I and Shin D H 1999 6H to 3C polytype transformation in silicon carbide *Japan. J. Appl. Phys.* 2 **38** L27
[53] Hallin C, Ellison A, Ivanov I G, Henry A, Son N T and Janzén E 1998 CVD growth and characterisation of SiC epitaxial layers on faces perpendicular to the (0001) basal plane *Mater. Sci. Forum* **264** 123
[54] Matsunami H, Kimoto T and Yano H 2000 Epitaxial growth of SiC on non-typical orientations and MOS interfaces *Mater. Res. Soc. Symp. Proc.* **640** 3.4
[55] Okojie R S, Xhang Ming, Pirouz P, Tumakha S, Jessen G and Brillson L J 2001 Observation of 4H-SiC to 3C-SiC polytypic transformation during oxidation *Appl. Phys. Lett.* **79** 3056
[56] Okojie R S, Xhang M, Pirouz P, Tumakha S, Jessen G and Brillson L J 2002 4H- to 3C-SiC polytypic transformation during oxidation *Mater. Sci. Forum* **389–393** 451
[57] Dombrowski K F, Kaufman U, Kunzer M, Maier K, Schneider J, Shields V B and Spencer M G 1994 Deep donor state of vanadium in cubic silicon carbide (3C-SiC) *Appl. Phys. Lett.* **65** 1811
[58] Evwaraye A O, Smith S R and Mitchel W C 1995 Determination of the band offsets of the 4H-SiC/6H-SiC heterojunction using the vanadium donor (0/+) level as a reference *Appl. Phys. Lett.* **67** 3319
[59] Harris G L (ed) 1995 *Properties of Silicon Carbide* (London: INSPEC)
[60] Choyke W J, Hamilton D R and Patrick L 1964 Optical properties of cubic SiC: luminescence of nitrogen–exciton complexes, and interband absorption *Phys. Rev.* A **133** 1163
[61] Tumakha S, Brillson L J and Okojie R S, Defect formation in 4H-SiC annealed in UHV, unpublished
[62] Brillson L J, Tumakha S, Jessen G H, Okojie R S, Zhang M and Pirouz P 2002 Thermal and doping dependence of 4H-SiC polytype transformation *Appl. Phys. Lett.* **81** 2785
[63] Panknin D, Wirth H, Mücklich A and Skorupa W 2001 Electrical and microstructural properties of highly boron-implantion doped 6H-SiC *J. Appl. Phys.* **89** 3162
[64] Pirouz P, Demenet J L and Hong M H 2001 On transition temperatures in the plasticity and fracture of semiconductors *Phil. Mag.* A **81** 1207
[65] Okojie R S, Zhang M, Pirouz P, Brillson L J, Tumakha S and Jessen G H 2002 Doping and temperature effects on strain in n-type 4H-SiC epilayers *Proc. Electronic Materials Conf.* (Warrendale, PA: TMS) p 73
[66] Miao M S, Limpijumnong S and Lambrecht W R L 2001 Stacking fault band structure in 4H-SiC and its impact on electronic devices *Appl. Phys. Lett.* **79** 4360
[67] Iwata H, Lindefelt U, Öberg S and Briddon P R 2002 Localized electronic states around stacking faults in silicon carbide *Phys. Rev.* **65** 033203
[68] Liu J Q, Chung H J, Kuhr T, Li Q and Skowronski M 2002 Structural instability of 4H-SiC polytype induced by n-type doping *Appl. Phys. Lett.* **80** 2111
[69] Kuhr T A, Liu J, Chung H J, Skowronski M and Szmulowicz F 2002 Spontaneous formation of stacking faults in highly doped 4H-SiC during annealing *J. Appl. Phys.* **92** 5863
[70] Bergman J P, Lendenmann H, Nilsson P Å, Lindefelt U and Skytt P 2001 Crystal defects as source of anomalous forward voltage increase of 4H-SiC diodes *Mater. Sci. Forum* **353** 299
[71] Stahlbush R E and MacFarlane P J 2001 Light emission from interface traps and bulk defects in SiC MOSFETs *J. Electron. Mater.* **30** 188

[72] Galeckas A, Linnros J, Breitholtz B and Bleichner H 2001 Application of optical emission microscopy for reliability studies in 4H-SiC p+/n–/n+ diodes *J. Appl. Phys.* **90** 980
[73] Galeckas A, Linnros J and Pirouz P 2002 Recombination-enhanced extension of stacking faults in 4H-SiC p–i–n diode under forward bias *Appl. Phys. Lett.* **81** 883
[74] Sridhara S G, Clemen L L, Devaty R P, Choyke W J, Larkin D J, Kong H S, Troffer T and Pensl G 1998 Photoluminescence and transport studies of boron in 4H SiC *J. Appl. Phys.* **83** 7909
[75] Weeks J D, Tully J C and Kimerling L C 1975 Theory of recombination-enhanced defect reactions in semiconductors *Phys. Rev.* B **12** 3286
[76] Maeda K and Takeuchi S 1996 *Dislocations in Solids* ed F R N Nabarro and M S Duesbery (Amsterdam: North-Holland) chapter 10, p 443
[77] Skromme B J, Palle K, Bryant L R, Meidia H, Mahajan S, Poweleit C D, Vetter W M, Dudley M, Moore K and Gehoski T 2002 Processing-induced polytype transformation in heavily n-doped 4H-SiC *Proc. Electronic Materials Conf.* (Warrendale, PA: TMS) p 75
[78] Skromme B J, Palle K C, Mikhov M K, Meidia H, Mahajan S, Huang X R, Vetter W M, Dudley M, Moore K, Smith S and Gehoski T 2003 Effects of structural defects on diode properties in 4H-SiC *Silicon Carbide 2002—Materials, Processing and Devices* (*MRS Proc.* vol 742) ed S E Saddow, D J Larkin, N S Saks, A Schoener and M Skowronski (Warrendale, PA: Materials Research Society) at press
[79] Zimmerman U, Osterman J, Galeckas A and Hallen A 2003 SEM visibility of stacking faults in 4H-silicon carbide epitaxial and implanted layers *Mater. Sci. Forum* submitted
[80] Liu J Q, Skowronski M, Hallin C, Söderholm R and Lendenmann H 2002 Structure of recombination-induced stacking faults in high-voltage SiC p–n junctions *Appl. Phys. Lett.* **80** 749
[81] Skromme B J, Palle K, Poweleit C D, Bryant L R, Vetter W M, Dudley M, Moore K and Gehoski T 2002 Oxidation-induced crystallographic transformation in heavily n-doped 4H-SiC wafers *Mater. Sci. Forum* **389–393** 455
[82] Tumakha S, Brillson L J and Okojie R S Temperature-dependent photoluminescence and cathodoluminescence spectroscopies of highly-doped 4H-SiC, unpublished
[83] Kakanakova-Georgieva A, Yakimova R, Linnarsson M K and Janzén E 2002 Site-occupying behavior of boron in compensated p-type 4H-SiC grown by sublimation epitaxy *J. Appl. Phys.* **91** 3471
[84] Kakanakova-Georgieva A, Yakimova R, Henry A, Linnarsson M K, Syväjärvi M and Janzén E 2002 Cathodoluminescence identification of donor–acceptor related emissions in as-grown 4H-SiC layers *J. Appl. Phys.* **91** 2890
[85] Hallin C, Konstantinov A O, Pécz B, Kordina O and Janzén E 1997 The origin of 3C polytype inclusions in epitaxial layers of silicon carbide grown by chemical vapour deposition *Diamond Relat. Mater.* **6** 1297
[86] Zhou W L, Pirouz P and Powell J A 1998 The origin of triangular surface defects in 4H-SiC CVD epilayers *Mater. Sci. Forum* **264–268** 417
[87] Sridhara S G, Carlsson F H C, Bergman J P and Janzén E 2001 Luminescence from stacking faults in 4H-SiC *Appl. Phys. Lett.* **79** 3944
[88] Bai S, Wagner G, Shishkin E, Choyke W J, Devaty R P, Zhang M and Pirouz P 2001 Spectra associated with stacking faults in 4H SiC grown in a hot wall CVD reactor *ICSCRM 2001* (abstract) (Zurich: Trans Tech Publications)
[89] Iwata H, Lindefelt U, Öberg S and Briddon P R 2002 Theoretical study of cubic polytype inclusions in 4H-SiC *Mater. Sci. Forum* **389–393** 533
[90] Waldrop J R, Grant R W, Wang Y C and Davis R F 1992 Metal Schottky barrier contacts to alpha 6H-SiC *J. Appl. Phys.* **72** 4757